Coaxial Nested Couplers-Based Offset-Tolerance Rotary Wireless Power Transfer Systems for Electric Excitation Motors

LONGYANG WANG, JIANGUI LI, HUI NIE, JINCHENG LIU, AND SHAOXING KE
School of Mechanical and Electronic Engineering, Wuhan University of Technology, Wuhan 430070, China

Corresponding author: Jiangui Li (jianguili@whut.edu.cn)

ABSTRACT In order to improve poor anti-offset capability of rotary transformer in electric excitation motor, a coaxial nested rotary wireless power transfer (CNR-WPT) system has been proposed in this paper. Firstly, considering the spatial geometric relationship of the coils and the power transmission efficiency of the CNR-WPT, the preliminary coil structure has been proposed. Secondly, through theoretical derivation, the specific relationship between the mutual inductance of the coils and the offset have been studied to verify the feasibility of the preliminary design. Thirdly, aiming at the problem that the CNR-WPT is susceptible to steel interference, the magnetic field has been optimized by adding ferrite and introducing a protective casing in this paper. Finally, an experimental platform for CNR-WPT system has been built. The experimental results verify that the power transmission efficiency of the CNR-WPT system can reach 90% when the radial offset and axial offset are below 5 mm, and the angular offset is below 5°. The energy losses can be reduced by adding ferrite and protecting the casing. The CNR-WPT system thereof can also be applied to other rotary power transmission occasions.

INDEX TERMS Electric excitation motor, coaxial nested rotary wireless power transfer system, anti-offset capability, power transmission efficiency.

I. INTRODUCTION

Due to its simple design and low cost, the electric excitation motor is widely used in industrial manufacturing, aerospace and other fields [1], [2]. Electric excitation motors require brushes and slip rings to power the rotor of the motor, causing a large amount of friction loss, and at the same time, sparks are easily generated, increasing safety hazards [3], [4]. Therefore, some scholars have used a rotary transformer to power the rotor of the electric excitation motor [1], [3]–[7].

Reference [1] has derived the calculation method of air gap and stator core size of three-phase rotary transformer, and the equation for magnetic coupling coefficient, which provided guidance and reference for the optimal design of three-phase rotary transformer. Reference [5] has proposed an optimization method for a rotary transformer, and a rotary transformer has been designed according to this method. Finally, the transformer has been verified by simulation. Reference [6] has described the advantages of using a rotary transformer instead of brushes and slip rings, and tested the

The associate editor coordinating the review of this manuscript and approving it for publication was Giambattista Gruosso.

performance of a 90kW brushless doubly-fed motor based on a rotary transformer, as shown in Fig. 1. The experimental results confirmed that the overall performance has been improved and this motor is prospective in terms of application. Reference [7] has proposed a rotary transformer based on a pot core geometry, as shown in Fig. 2. The rotary transformer has significant optimization compared with conventional ones.

In summary, many scholars have carried out research on rotary transformers and have achieved certain research results. Whereas the rotary transformer brings benefits, it also has certain defects, mainly reflected in the following two points. First, the stator core of the rotary transformers is a laminated silicon steel sheet [6], which leads to a complicated manufacturing process and a high production cost. Second, in general, the rotary transformers have a low working frequency [1], [5]–[7]. The low frequency characteristic makes us unable to design the working air gap of the rotary transformers too large, otherwise it will cause an increase of magnetic flux leakage, which will result in an increased magnetic loss and consequently a reduction in efficiency [1]. In the case of motor shaft vibration, a small working air
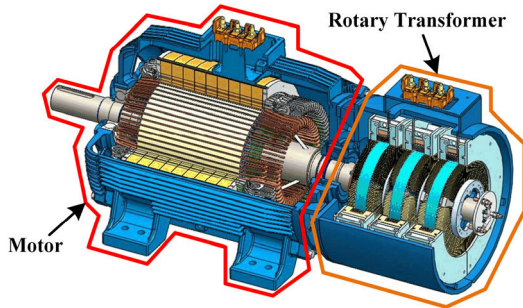
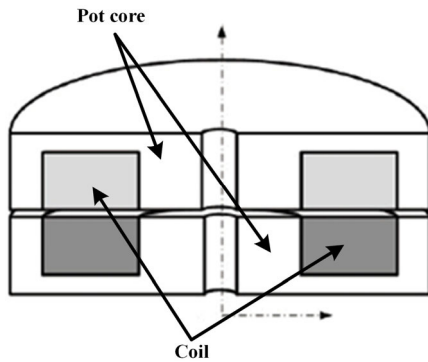**FIGURE 1.** Doubly fed three-phase induction machine with a rotary transformer.

FIGURE 2. The rotary transformer based on a pot core geometry.

gap results in a higher probability of the rotary transformers jamming, which affects the normal operation of the motor. In conclusion, the rotary transformer has higher requirements for the design and manufacturing process, and its anti-offset capability is poor, which will fail to meet the requirements needed to normally operate in harsh conditions.

As an ideal power transmission method, wireless power transfer system can transmit power from the power supply side to the equipment side under non-contact conditions [8]–[11]. Because of its advantages of safety, reliability and flexibility, it is widely used in various power transmission processes, such as mobile phone charging, electric vehicle charging, drone charging, etc., [12]–[14]. Some achievements have been made in the research of the application of WPT systems in the electric excitation motor. Reference [15] designed a contactless maglev rotating power transfer system with new rotary inductive coupled structure for the testing equipment on shaft of high-speed rotation applications. The maximum output power received in load is 297W and the maximum efficiency is about 82%. Reference [16] proposed a new type of in-wheel outer rotor switched reluctance motor (ORSRM) drive based on selective wireless power transfer (WPT) using receivers of different resonant frequencies. Finally, the simulation results proved the feasibility of this wireless ORSRM drive. Reference [17] proposed a wireless power transfer (WPT) system to realize brushless electrically excited synchronous motor (EESM), and the correctness of the system was verified by experiment and simulation.
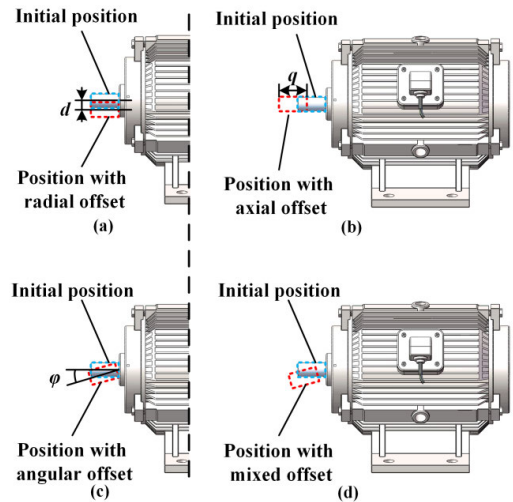

FIGURE 3. The schematic diagram of the offset conditions. (a) Radial offset. (b) Axial offset. (c) Angular offset. (d) Mixed offset.

In conclusion, although some achievements have been made, scholars have not made a profound study about the position relationship between stator and rotor. In this paper, the wireless power transmission technology is applied to the electric excitation motor, and a coaxial nested rotary wireless power transfer (CNR-WPT) system has been proposed. The power transmission efficiency of the CNR-WPT system can be guaranteed, in the case of a large working air gap. Therefore, it is ensured that in case of motor shaft vibration, the stationary side coil and the rotary side coil do not interfere with each other, which reduces the possibility of the motor stalling. At the same time, in view of the problem that steel easily interferes with the normal operation of the CNR-WPT system, the magnetic field has been optimized by adding ferrite, and a protective casing has been designed, in this paper.

II. VIBRATION ANALYSIS AND STRUCTURE
A. VIBRATION ANALYSIS OF MOTOR SHAFT
In the actual application process, the motor shaft may vibrate irregularly, due to irresistible factors such as unreasonable design, load change, external interference, etc., [18], [19]. For the purposes of this paper, the vibration process is simplified to different offsets of the motor shaft at multiple fixed times. The following four offset situations may occur on the motor shaft, namely, radial offset only, axial offset only, angular offset only, and mixed offset, as shown in Fig. 3 (a), Fig. 3 (b), Fig. 3 (c), and Fig. 3 (d), respectively. Mixed offset refers to the circumstances where two or three offset conditions occur at the same time.

In Fig. 3, d is the radial offset degree, q is the axial offset degree, and φ is the angular offset degree. This paper takes the above offsets into account when designing the CNR-WPT system for 1kW electric excitation motor. Table 1 contains the required parameters of the CNR-WPT system.

B. STRUCTURE OF CNR-WPT
It is shown the three-dimensional model and the simplified diagram of CNR-WPT system in Fig.4 (a) and Fig. 4 (b), respectively. The CNR-WPT system consists of

TABLE 1. Requirements of CNR-WPT system.

Description	Symbol	Value
Radial offset tolerance	d_t	4 mm
Axial offset tolerance	q_t	4 mm
Angular offset tolerance	φ_t	4 °
Transmission efficiency	η	85 %
Transmission power	P	30 W – 50W

(a)

(b)
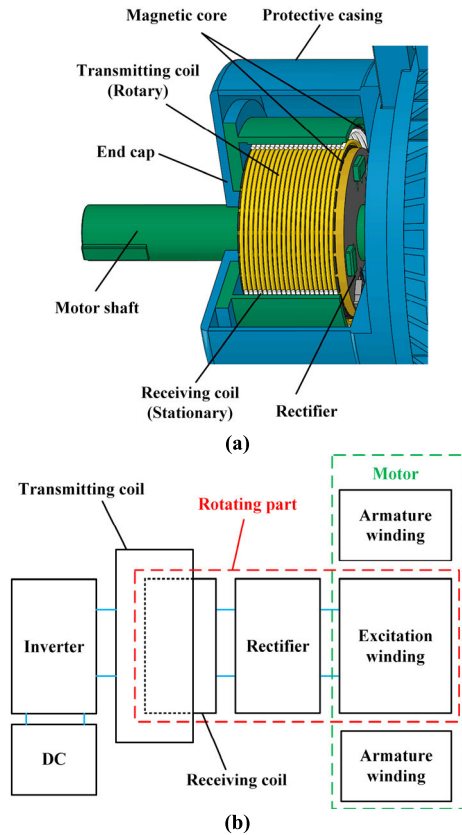
FIGURE 4. The structure of CNR-WPT. (a) The three-dimensional model. (b) The simplified diagram.

transmitting coil, receiving coil, inverter, rectifier, DC power, protective casing and end cap. The transmitting coil is fixed on the end cap and is connected with the inverter output. The DC power output is connected with the input of the inverter. The DC power and inverter are not shown in Fig. 4 (a). The receiving coil and rectifier are fixed on the motor shaft. The input of the rectifier is connected to the receiving coil, and the output is connected with the excitation winding of the motor.

During operation, the receiving coil is stationary and the transmitting coil is in a rotating state. After current flows out from the DC power, it changes into a high-frequency alternating current through the inverter, then passes through two coils to the rectifier, and finally turns into a direct current through the rectifier to supply the excitation winding of the motor.

III. COIL DESIGN
A. SIZE AND POSITION CONSTRAINTS OF THE COILS
The wireless power transfer [8]–[14] has two classic coil topologies: 1) planar spiral coils; 2) coaxial spiral coils.

TABLE 2. Transmitting coil parameters of the CNR-WPT system.

Parameter	Value
Transmitting coil turns	20
Transmitting coil diameter	101.7 mm
Transmitting coil height	43.5 mm
Wire cross-sectional area	1.508 mm²
Transmitting coil material	Litz wire
The diameter of each core line of the Litz wire	0.04 mm
The number of the core lines	1200

A coaxial spiral coil has a smaller diameter than a planar spiral coil. At the same speed, the coaxial spiral coil is subjected to less centrifugal force, so a wireless power transfer based on this coil has better stability. In this paper, a coaxial nested spiral coil is used for system design. The transmitting coil is on the outside and the receiving coil is on the inside.

When the magnetic flux density is constant, the magnetic flux is proportional to the cross-sectional area. Therefore, in designing the CNR-WPT system, in order to obtain a larger magnetic flux, the transmitting coil diameter needs to increase accordingly. However, due to cost and size constraints, the diameter of the transmitting coil cannot be increased indefinitely. Considering comprehensively, the parameters of transmitting coil that we have used in analyzation are shown in Table 2. Using this particular coil in the transmitting side, we proceeded to analyze the characteristics of the receiving coil.

This principle should be followed when designing the receiving coil: In case of motor shaft deviation, the receiving coil and the transmitting coil cannot interfere with each other. In practical applications, the offset of the motor shaft mostly exists in the form of mixed offset. For the convenience of observation, this paper uses a rectangle to represent the coil body, as shown in Fig. 5.

From Fig. 5, it can be obtained that the key factor determining whether the two coils interfere with each other is d and φ. Therefore, in order to ensure that there is no direct contact between the transmitting coil and the receiving coil when the offset occurs, the dimensions of coils should satisfy (1).

$$\cos(90^\circ - \arctan\frac{D_S}{H_S} - \varphi)(\sqrt{D_S^2 + H_S^2}) + 2d < D_P \quad (1)$$

where D_P is the diameter of transmitting coil, and D_S and H_S are the diameter and height of receiving coil, respectively. To analysis further, $D_{P.CAL}$ has been introduced in this paper, representing the calculation of the transmitting coil diameter, and the definition is given by,

$$\begin{cases} \cos(90^\circ - \arctan\frac{D_S}{H_S} - \varphi)(\sqrt{D_S^2 + H_S^2}) + 2d = D_{P.CAL} \\ D_{P.CAL} < D_P \end{cases}$$
$$(2)$$

The relationships between $D_{P.CAL}$, D_S and H_S at $\varphi = 2°$ and $d = 2$ mm, at $\varphi = 4°$ and $d = 4$ mm, and at $\varphi = 6°$ and $d = 6$ mm are shown in Fig. 6 (a), Fig. 6 (b), and Fig. 6 (c), respectively. It can be seen that the calculated values of
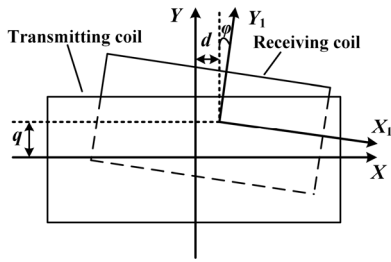
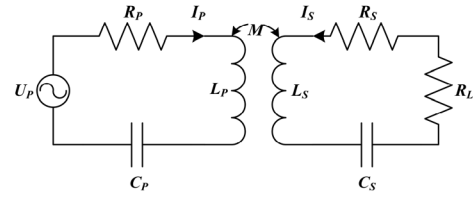**FIGURE 5.** The schematic diagram of the offset form.

(a)

(b)

(c)

FIGURE 6. The relationship between $D_{P.CAL}$, D_S and H_S at different offsets. (a) at $d = 2$ mm, $\varphi = 2°$. (b) at $d = 4$ mm, $\varphi = 4°$. (c) at $d = 6$ mm, $\varphi = 6°$.

transmitting coil diameter are proportional to the receiving coil diameter and the receiving coil height, respectively, under the same offset, from Fig. 6. And in Fig. 6 (a), when the transmitting coil height ranges from 40mm to 50mm and the

FIGURE 7. The equivalent circuit diagram.

diameter ranges from 70mm to 90mm, the calculated values of the diameter of the transmitting coil are all below the actual value given above, at $\varphi = 2°$ and $d = 2$ mm. But at $\varphi = 4°$ and $d = 4$ mm, as shown in Fig. 6 (b), a few calculated values are higher than the actual value. In addition, at $\varphi = 6°$ and $d = 6$ mm, about one-third of the calculated values exceed the actual value, as shown in Fig. 6 (c).

In summary, with the premise that the transmitting coil is given, the diameter and height of the receiving coil should be reduced in order to tolerate a larger offset. For analytical convenience, the height of the receiving coil is equal to the height of transmitting coil in this paper.

B. EFFICIENCY CONSTRAINTS

The WPT system requires capacitors to compensate for the transmit and receive coils, respectively, to operate at the same frequency point. At present, there are four classic compensation structures: S-S, S-P, P-S, and P-P [20]. This paper chooses the S-S structure and its equivalent circuit is shown in Fig. 7.

In Fig. 7, L_P, L_S, R_P, R_S, C_P, and C_S are the inductance, internal resistance, and compensation capacitance of the transmitting coil and the receiving coil, respectively; R_L is the load resistance; I_P and I_S are the currents of the primary and secondary sides, respectively; U_P is the high-frequency voltage source; M is the mutual inductance of the transmitting and receiving coils. According to the Kirchhoff Laws, (3) can be deduced [11].

$$\begin{cases} U_P = Z_P I_P + j\omega I_S M \\ -j\omega I_P M = Z_S I_S \end{cases} \tag{3}$$

where ω is the operating frequency; Z_P and Z_S are the equivalent impedances of the primary and secondary circuits, respectively. And the variables can be calculated according to (4).

$$\begin{cases} Z_P = R_P + j\omega L_P + 1/j\omega C_P \\ Z_S = R_S + R_L + j\omega L_S + 1/j\omega C_S \end{cases} \tag{4}$$

When $j\omega L_P + 1/j\omega C_P = 0$ and $j\omega L_S + 1/j\omega C_S = 0$, the system transmission efficiency [14] can be calculated by (5).

$$\eta = \frac{\omega^2 M^2 R_L}{R_P(R_S + R_L)^2 + M^2\omega^2(R_S + R_L)} \tag{5}$$

In (6), R_P and R_S can be calculated by Law of Resistance. Fig. 8 shows the relationship between mutual inductance and transmission efficiency under different values of R_L,
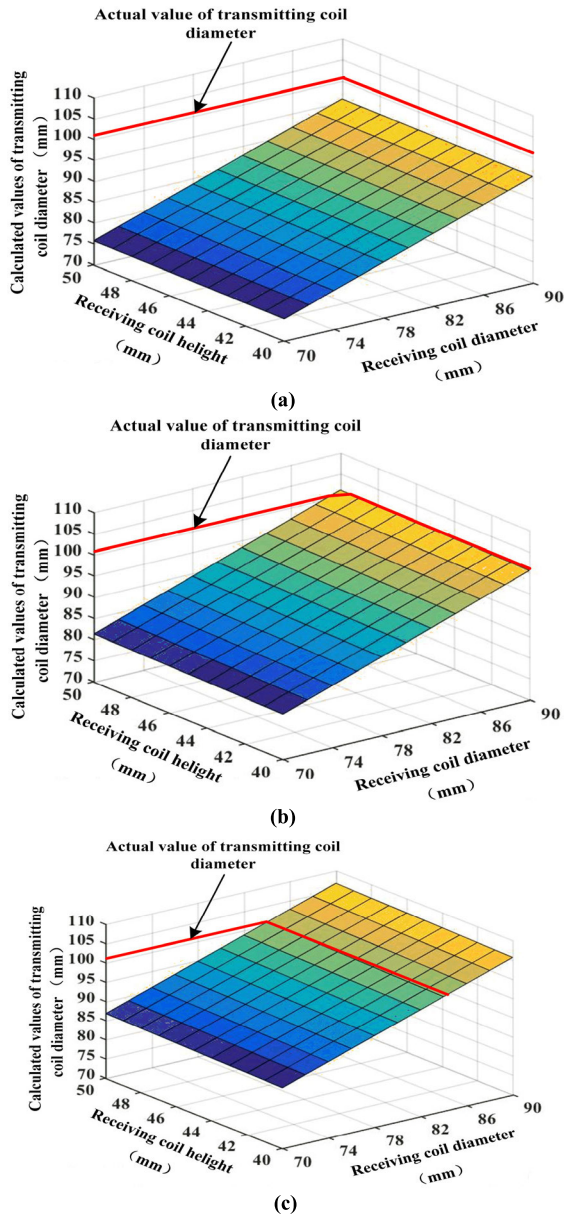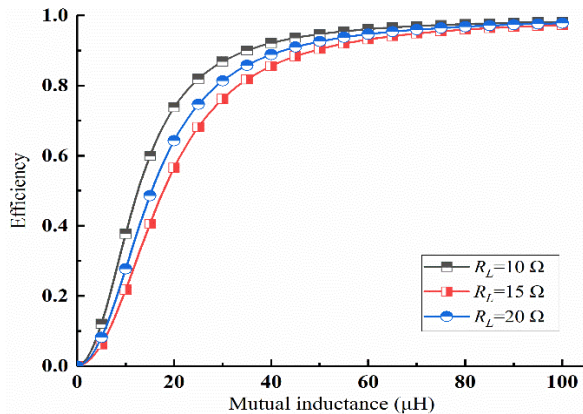
FIGURE 8. The relationship between η and M at different R_L.

FIGURE 9. The simplified schematic diagram of transmitting coil and receiving coil.
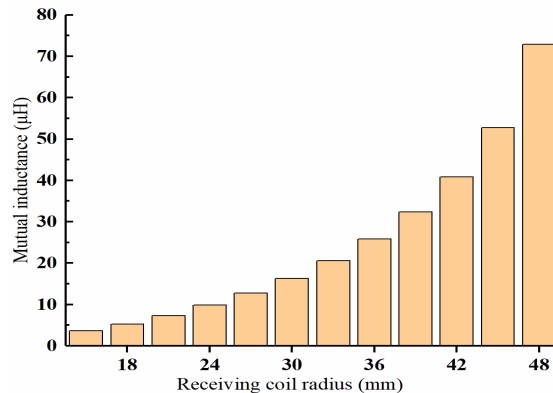

FIGURE 10. The relationship between r_S and M under given circumstances.

TABLE 3. The receiving coil parameters of the CNR-WPT system.

Parameter	Value
Receiving coil turns	20
Receiving coil diameter	76.9 mm
Receiving coil height	43.5 mm
Wire cross-sectional area	1.508 mm2
Receiving coil material	Litz wire
The diameter of each core line of the Litz wire	0.04 mm
The number of the core lines	1200

where N_P and N_S are the turns of the two coils respectively; r_P and r_S are the radii of the transmitting coil and the receiving coil, respectively; α is the angle between the line connecting the minimum calculation unit of the transmitting coil to the coordinate origin of the plane coordinate system of the transmitting coil and the X-axis of the coordinate system; β is the angle between the line connecting the minimum calculation unit of the receiving coil to the coordinate origin of the plane coordinate system of the receiving coil and the X-axis of the coordinate system.

Fig. 10 shows the relationship between the radius of the receiving coil and the mutual inductance under the given circumstances. It can be obtained that the mutual inductance increases in proportion to the augment of the radius of the receiving coil. In conclusion, in order to enhance the efficiency of the CNR-WPT system, it is necessary to increase the receiving coil radius.

Considering the coils' size and position limitations and power transmission efficiency, the receiving coil parameters of the CNR-WPT system in this paper are given in Table 3.

IV. ANTI-OFFSET CAPABILITY VERIFICATION

The previous chapter completed the preliminary design of the CNR-WPT system coils. In this chapter, the coils are theoretically analyzed to verify whether it can meet the anti-offset requirements. From (5) and (6), we can know that, the relationship between mutual inductance and offset has to be analyzed to make sure the coil can meet the anti-offset requirement.

The mutual inductance of coils with different conditions of offsets respectively have been calculated. For convenience,
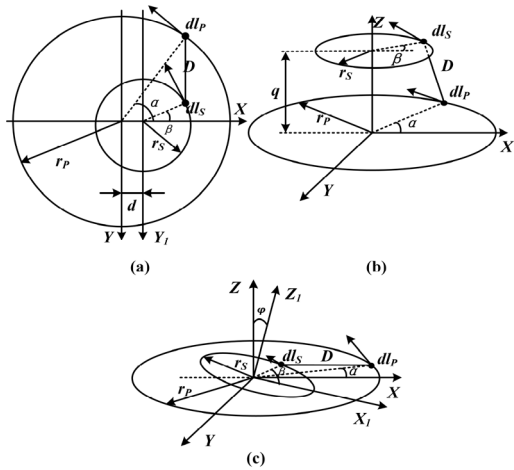
at $\omega = 100$ kHz. From Fig. 8, it can be known that, in the case of a fixed R_L, mutual inductance should be increased accordingly to improve the transmission efficiency. Mutual inductance between two single-turn coils can be calculated by Neumann's Formula [13], [21],

$$M = \frac{\mu_0}{4\pi} \times \oint \oint \frac{dl_P dl_S}{D} \tag{6}$$

where dl_P and dl_S are the minimum calculation units of the two coils respectively; μ_0 is the vacuum permeability; D is the distance between the two minimum calculation units. For convenience, in this paper, the turns of the receiving coil are equal to that of the transmitting coil.

The transmitting coil and the receiving coil of the CNR-WPT system have same axis. For convenience, the positional relationship of two single-turn coils is employed to represent that of the whole, as shown in Fig. 9. Thus, the mutual inductance of coils can be obtained by (7).

$$\begin{cases} M_0 = \frac{N_P N_S \mu_0}{4\pi} \times \int_0^{2\pi} \int_0^{2\pi} \frac{F}{D} d\alpha d\beta \\ F = r_P r_S (\cos\alpha\cos\beta + \sin\alpha\sin\beta) \\ D = \left[r_P^2 + r_S^2 - 2r_P r_S (\cos\alpha\cos\beta + \sin\alpha\sin\beta) \right]^{\frac{1}{2}} \end{cases} \tag{7}$$

FIGURE 11. The schematic diagram of the positional relationship of two coils under a singular offset. (a) The radial offset. (b) The axial offset. (c) The angular offset.

the single-turn coils have been taken into consideration. The position of the coils with radial offset, axial offset, and angular offset are shown in Fig. 11 (a), Fig. 11 (b), and Fig. 11 (c), respectively.

As shown in Fig. 11 (a), with only a radial offset between the transmitting coil and the receiving coil, i.e. $d \neq 0$ mm, the mutual inductance can be calculated by (8).

$$
\begin{cases}
M_1 = \dfrac{N_P N_S \mu_0}{4\pi} \times \displaystyle\int_0^{2\pi} \int_0^{2\pi} \dfrac{F}{D} d\alpha d\beta \\
F = r_P r_S (\cos\alpha\cos\beta + \sin\alpha\sin\beta) \\
D = [r_P^2 + r_S^2 + d^2 + 2dr_S\cos\beta - 2dr_P\cos\alpha \\
\quad -2r_P r_S(\cos\alpha\cos\beta + \sin\alpha\sin\beta)]^{\frac{1}{2}}
\end{cases}
\tag{8}
$$

As shown in Fig. 11 (b), with only an axial offset between two coils, i.e. $q \neq 0$ mm, the mutual inductance can be calculated by (10).

$$
\begin{cases}
M_2 = \dfrac{N_P N_S \mu_0}{4\pi} \times \displaystyle\int_0^{2\pi} \int_0^{2\pi} \dfrac{F}{D} d\alpha d\beta \\
F = r_P r_S (\cos\alpha\cos\beta + \sin\alpha\sin\beta) \\
D = \left[r_P^2 + r_S^2 + q^2 - 2r_P r_S(\cos\alpha\cos\beta + \sin\alpha\sin\beta) \right]^{\frac{1}{2}}
\end{cases}
\tag{9}
$$

As shown in Fig. 11 (c), with only angular offset between two coils, i.e. $\varphi \neq 0°$, the mutual inductance can be calculated by (11).

$$
\begin{cases}
M_3 = \dfrac{N_P N_S \mu_0}{4\pi} \times \displaystyle\int_0^{2\pi} \int_0^{2\pi} \dfrac{F}{D} d\alpha d\beta \\
F = r_P r_S (\cos\alpha\cos\beta + \sin\alpha\sin\beta\cos\varphi) \\
D = \left[r_P^2 + r_S^2 - 2r_P r_S(\cos\alpha\cos\beta\cos\varphi + \sin\alpha\sin\beta) \right]^{\frac{1}{2}}
\end{cases}
\tag{10}
$$

The relationships between mutual inductance and radial offset and axial offset are shown respectively in Fig. 12 (a) and the relationship between mutual inductance and angular offset is shown in Fig. 12 (b). From Fig. 12, it can be obtained that:
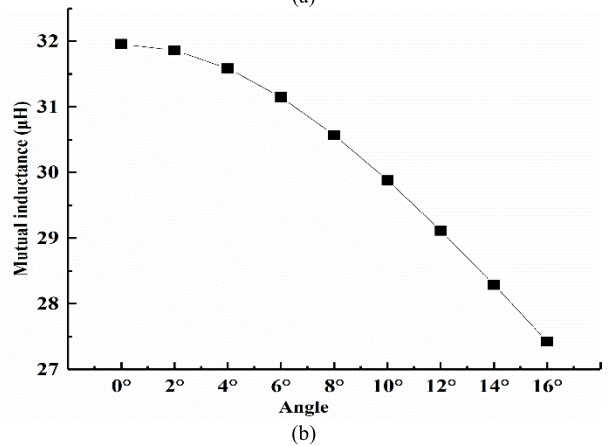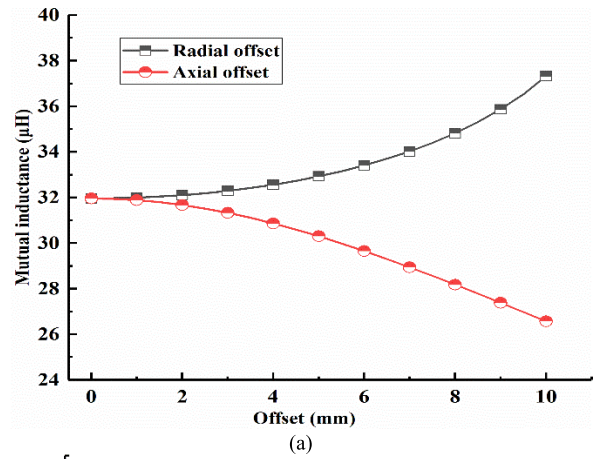

FIGURE 12. The relationship between mutual inductance and singular offset condition. (a) The radial offset and axial offset. (b) The angular offset.

1) As the radial offset increases, the mutual inductance gradually increases. When the offset is below 5 mm, the mutual inductance gradient is minimal. When the offset exceeds 5 mm, the mutual inductance gradient increases. The mutual inductance reaches 37.8 μH, when reaching 10 mm.

2) The mutual inductance decreases with the increase of the axial offset. When the offset is below 5 mm, the mutual inductance decreases slowly. The mutual inductance begins to decrease rapidly, when the offset exceeds 5 mm. When it reaches 10 mm, the mutual inductance drops to 26.6 μH.

3) For the angular offset, when the offset is below 4 °, the mutual inductance is basically constant. When the offset exceeds 4 °, the mutual inductance begins to drop rapidly, and when the offset reaches 16 °, the mutual inductance drops to 27.4 μH. Fig. 12 (b) shows the relationship between the angular offset and the mutual inductance.

By deducing the mutual inductance calculation equations of coils under singular offset condition, we have roughly understood the influence of the offset on the mutual inductance. But in reality, the offsets are often mixed, as shown in Fig. 13. Therefore, it is of more practical
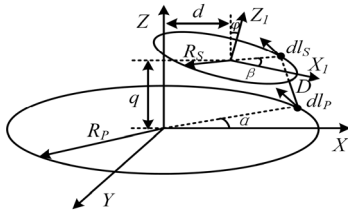
FIGURE 13. The schematic diagram of the position relationship of two coils when the mixed offset occurs.

significance to derive the calculation formula of mutual inductance when the mixed offset occurs.

When the radial offset, axial offset, and angular offset exist simultaneously, the mutual inductance between the two coils can be calculated by (11).

$$
\begin{cases}
M_4 = \dfrac{N_P N_D \mu_0}{4\pi} \times \displaystyle\int_0^{2\pi} \int_0^{2\pi} \dfrac{F}{D} d\alpha d\beta \\[2mm]
F = r_P r_S (\cos\alpha \cos\beta + \sin\alpha \sin\beta \cos\varphi) \\[1mm]
D = [r_P^2 + r_S^2 + d^2 + q^2 + 2dr_S \cos\beta \cos\varphi \\[1mm]
\quad\ -2dr_P \cos\alpha - 2r_P r_S(\cos\alpha \cos\beta \cos\varphi + \sin\alpha \sin\beta) \\[1mm]
\quad\ -2r_S q \cos\beta \sin\varphi]
\end{cases}
\tag{11}
$$

Fig.14 shows the relationship between mutual inductance and mixed offset degree. It can be obtained that when the radial offset and the axial offset are between 0-4 mm and the angular offset is between 0-4°, the mutual inductance is kept above $30\mu H$. According to Fig. 8, when the mutual inductance exceeds $30\mu H$, the transmission efficiency can be maintained at 80% or even more. In summary, the coils designed in the previous chapter can meet the anti-offset requirements.

V. DESIGN OF MAGNETIC SHIELDING

When a magnetic conducting material exists in the working environment of the CNR-WPT system, an eddy current effect will occur internally, resulting in energy loss. Ultimately, the transmission efficiency is reduced. The eddy current loss of cylindrical metal can be calculated by (12) [22].

$$
P_L = \frac{\pi l r^4 \omega^2 B_A^2}{32\rho}
\tag{12}
$$

where P_L is the eddy current loss; l is the metal length; r is the metal diameter; ω is the frequency; B_A is the metal internal magnetic flux density; ρ is the metal resistivity. From (13), it can be known that the eddy current loss of metal increases exponentially with the increase of magnetic flux density. Therefore, analyzing the change of magnetic flux density is the key to study the internal eddy current loss.

To analyze the change in magnetic flux density with magnetic conducting material approaching, a simulation model is built by placing a cylindrical steel on one side of the coil, as shown in Fig. 15. In this paper, $l = 65$ mm, $r = 10$ mm, and $s = 10$ mm.
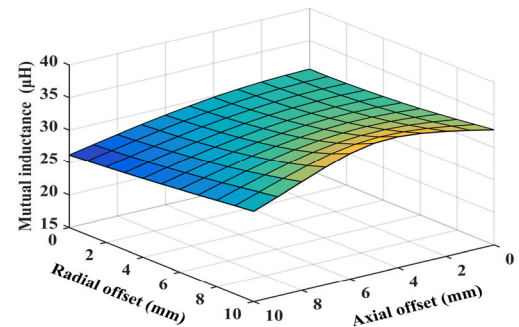
A finite element software was used to analyze the changes of magnetic field before and after the steel was introduced, as shown in Fig. 16 (a) and Fig. 16 (b), respectively.
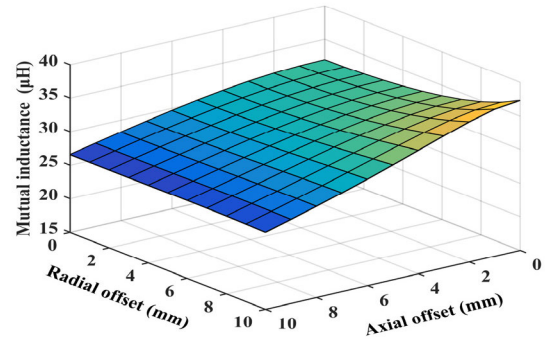
(a)
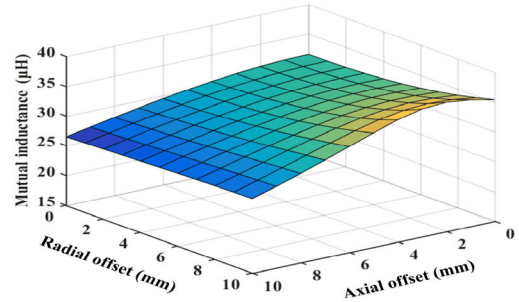
(b)

(c)

FIGURE 14. The relationship between M_4, d and q at different φ. (a) at $\varphi = 0°$. (b) at $\varphi = 2°$. (c) at $\varphi = 4°$.
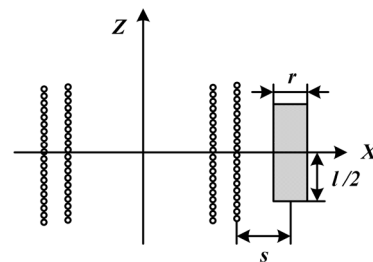

FIGURE 15. The simulation model with steel.

From the Fig. 16, it can be obtained that after the steel is introduced, the magnetic flux density of steel increases significantly, the maximum is about 1.55×10^{-2} T.

In this paper, the placement of ferrite around the coil is used to optimize the magnetic field to reduce the impact of the steel on the CNR-WPT system. The ferrite arrangement is shown in Fig. 17.

After the addition of ferrite, the magnetic field distribution of the system is shown in Fig. 18. It can be
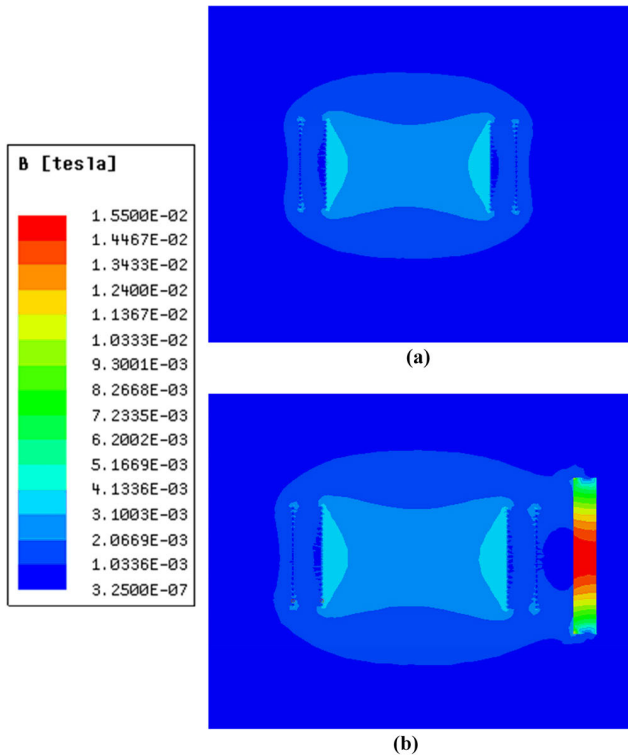
FIGURE 16. The changes of magnetic field (a) without steel interference. (b) with steel interference.
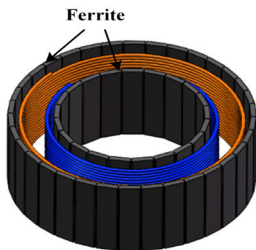

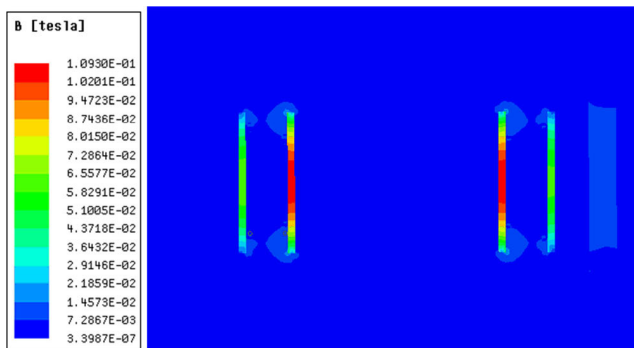FIGURE 17. The ferrite core arrangement.

FIGURE 18. The magnetic field distribution with ferrite added.

seen that the magnetic flux density of the steel reduced to 1.01×10^{-2} T. Comparing with no-ferrite topology, the magnetic flux density is significantly reduced.

From the above analysis, a conclusion can be reached that the magnetic field optimization can reduce the influence of
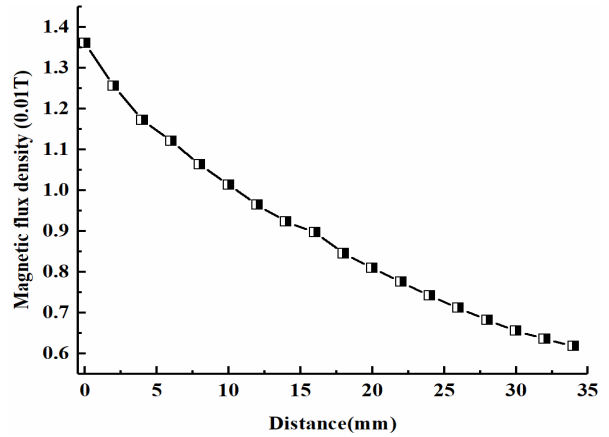

FIGURE 19. The change of magnetic flux density caused by steels of different distances.
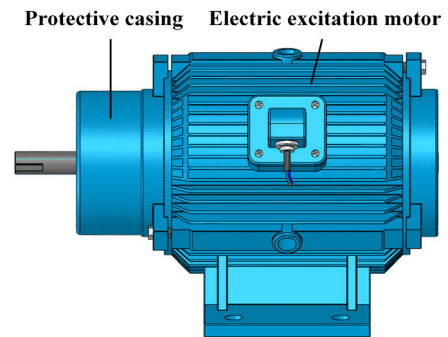

FIGURE 20. The schematic diagram of aluminum alloy protective casing.
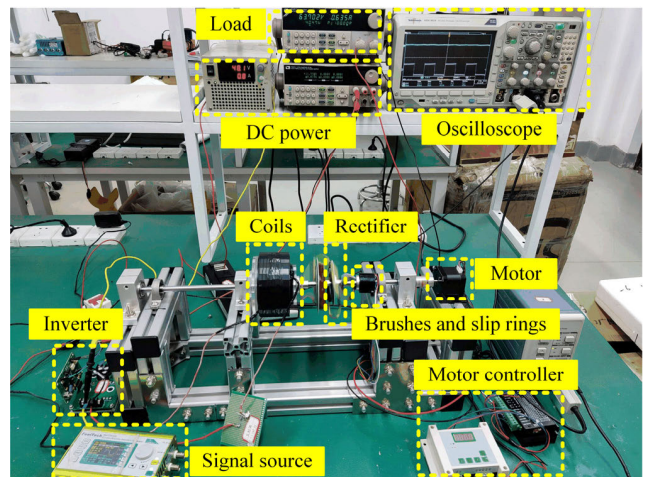
FIGURE 21. The experiment platform for CNR-WPT.

steel interference on the system, but there is still residual energy loss. This paper discusses the relationship between the location of steel and the performance of the CNR-WPT system to find out the minimum range of steel placements around the system, i.e. the maximum influence of steel interference, allowed to maintain normal operation. Then, by installing an aluminum alloy protective casing, the steel is restricted outside this range, thereby further reducing energy loss.

TABLE 4. The experiment parameters of the CNR-WPT system.

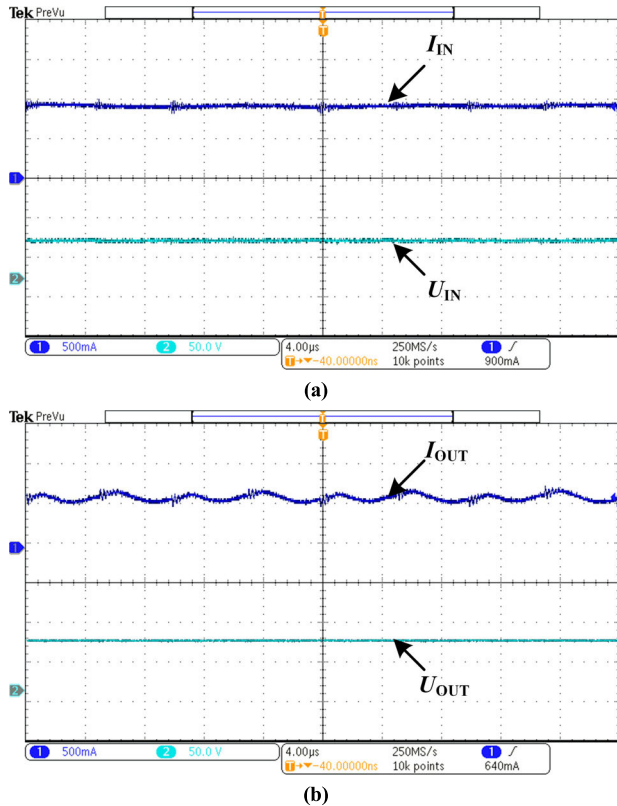| Parameter	Value
Self-inductance of transmitting coil	109.8 μH
Self-inductance of receiving coil	104.8 μH
Mutual inductance without offset	90.7 μH
Frequency	100 kHz
Load resistance	100 Ω
Revolutions per minute	500

FIGURE 22. The measured waveform without any offset. (a) The input waveform. (b) The output waveform.
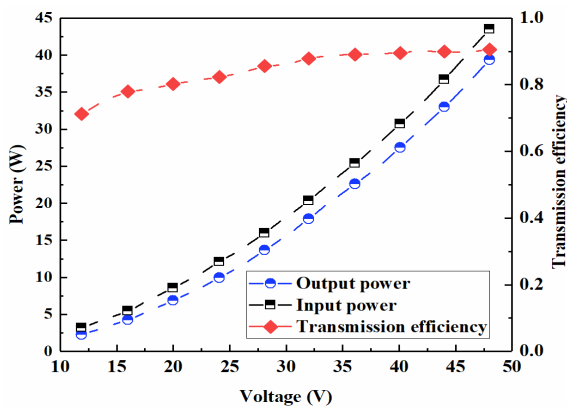

FIGURE 23. The relationship between transmission efficiency and transmission power.

The effect of steels at different distances to coils has been analyzed by finite element software, and the results are shown in Fig. 19.
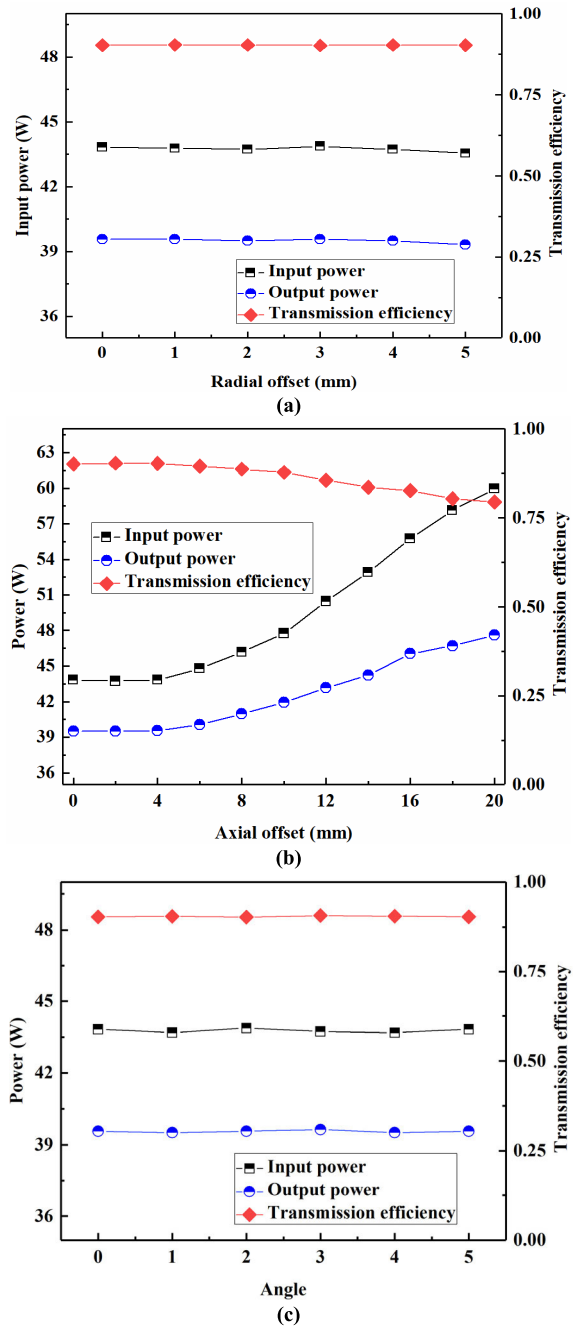
FIGURE 24. The relationship between transmission efficiency and singular offset condition. (a) radial offset. (b) axial offset. (c) angular offset.

From Fig. 19, it is clearly shown that as the steel is gradually moved away, the magnetic flux density is gradually decreased. When the distance reaches 30 mm, the magnetic flux density of the steel decreases to 6.55×10^{-3} T.

Considering energy loss and size of the aluminum alloy protective casing, a 30 mm casing has been introduced in this paper, ensuring that no steel comes closer than 30 mm, thereby effectively controlling energy loss. The aluminum alloy protective casing is shown in Fig. 4 (a) and Fig. 20.
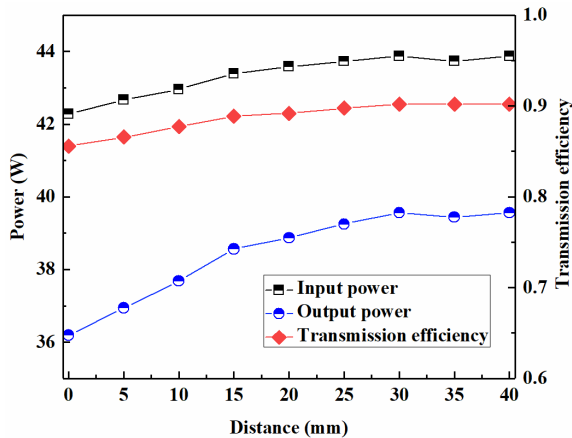
FIGURE 25. The change of efficiency and power caused by steel of different distances.

VI. EXPERIMENT

An experiment platform is built to measure the performance of CNR-WPT system, as shown in Fig. 21. Table 4 shows the detailed parameters of the experiment.

Fig. 22 shows the measured waveform without any offset. It could be clearly seen that the input voltage U_{IN} is constant about 47.9 V, and the input current I_{IN} is constant about 0.914 A. The output voltage U_{OUT} is about 62.8 V, and the output current I_{OUT} is about 0.631 A. Therefore, the transmission efficiency of CNR-WPT system under this condition is about 90.5%.

Fig. 23 shows the relationship between transmission efficiency and transmission power. With the increase of the DC voltage, the primary input power and the secondary output power rise in the same way. When the input voltage changes from 12 V to 38 V, the transmission efficiency maintains increasing, but the transmission efficiency growth rate remains unchanged. The transmission efficiency is kept around 90%, after the DC input voltage reaches 38 V.

The relationships between transmission efficiency and singular offset condition are shown in Fig. 24, respectively. Due to the special structure of CNR-WPT system, we are unable to achieve conditions when the radial offset is over 5 mm and the angular offset is over 5 °. It could be clearly seen that when the radial offset is below 5 mm, the axial offset is below 5 mm and the angular offset is below 5 °, the transmission efficiency remains basically unchanged respectively. It is important to note that when the axial offset exceeds 5 mm, the transmission efficiency begins to decrease, but the output power begins to rise. When the offset reaches 20 mm, the efficiency is reduced to 79.4%, and the output power is increased to 47.6 W.

Fig. 25 shows the changes of efficiency and power caused by steel of different distances. When the distance exceeds 25 mm, the output power and transmission efficiency of the CNR-WPT system are basically unaffected by the steel. However, the output power and transmission efficiency are reduced when the distance is below 25 mm. At a distance of 0 mm, the output power is reduced to 36.2 W and the transmission efficiency is reduced to 85.6%.

VII. CONCLUSION

A coaxial nested rotary wireless power transfer (CNR-WPT) system has been proposed in this paper to improve the poor anti-offset capability of the rotary transformer. Firstly, based on vibration analysis, the design requirements of CNR-WPT system have been analyzed. Then, considering spatial constraints and transmission efficiency, the preliminary design process of the coil was carried out. Then, theoretical analysis shows that the preliminary design of the coil can meet the design requirements. In order to reduce the influence of steel interference on CNR-WPT system, this paper optimizes the magnetic field by adding ferrite core and a protective casing has been introduced to minimize the interference with the magnetic object in the working environment. Finally, a CNR-WPT system experimental platform has setup to measure transmission efficiency and output power. The experimental results verify that:

1) The transmission efficiency of CNR-WPT system can be maintained above 90%, when the radial offset and axial offset are below 5 mm, and the angular offset is below 5°.
2) By introducing the ferrite and protecting the casing, energy losses can be reduced.

The CNR-WPT system thereof can also be applied to other rotary power transmission occasions.

REFERENCES

[1] H. Zhong, L. Zhao, and X. Li, "Design and analysis of a three-phase rotary transformer for doubly fed induction generators," *IEEE Trans. Ind. Appl.*, vol. 51, no. 4, pp. 2791–2796, Jul. 2015.

[2] P. Ledesma and J. Usaola, "Doubly fed induction generator model for transient stability analysis," *IEEE Trans. Energy Convers.*, vol. 20, no. 2, pp. 388–397, Jun. 2005.

[3] J. Legranger, G. Friedrich, S. Vivier, and J. C. Mipo, "Comparison of two optimal rotary transformer designs for highly constrained applications," in *Proc. IEEE Int. Electric Mach. Drives Conf.*, Antalya, Turkey, May 2007, pp. 1546–1551.

[4] K. D. Papastergiou and D. E. Macpherson, "Contact-less transfer of energy by means of a rotating transformer," in *Proc. IEEE Int. Symp. Ind. Electron. ISIE)*, Dubrovnik, Croatia, 2005, pp. 1735–1740.

[5] N. L. Zietsman and N. Gule, "Optimal design methodology of a three phase rotary transformer for doubly fed induction generator application," in *Proc. IEEE Int. Electric Mach. Drives Conf. (IEMDC)*, Coeur d'Alene, ID, USA, May 2015, pp. 763–768.

[6] M. Ruviaro, F. Runcos, N. Sadowski, and I. M. Borges, "Analysis and test results of a brushless doubly fed induction machine with rotary transformer," *IEEE Trans. Ind. Electron.*, vol. 59, no. 6, pp. 2670–2677, Jun. 2012.

[7] J. P. C. Smeets, L. Encica, and E. A. Lomonova, "Comparison of winding topologies in a pot core rotating transformer," in *Proc. 12th Int. Conf. Optim. Electr. Electron. Equip.*, May 2010, pp. 103–110.

[8] J. Wang, M. Hu, C. Cai, Z. Lin, L. Li, and Z. Fang, "Optimization design of wireless charging system for autonomous robots based on magnetic resonance coupling," *AIP Adv.*, vol. 8, no. 5, May 2018, Art. no. 055004.

[9] Z. Zhang, H. Pang, A. Georgiadis, and C. Cecati, "Wireless power Transfer—An overview," *IEEE Trans. Ind. Electron.*, vol. 66, no. 2, pp. 1044–1058, Feb. 2019.

[10] J. Wang, C. Cai, M. Long, K. Liu, and M. Sun, "Study of resonant self-charging rats experiment playground based on witricity technology," *Int. J. Appl. Electromagn. Mech.*, vol. 53, no. 3, pp. 409–421, Feb. 2017.

[11] C. Cai, J. Wang, Z. Fang, P. Zhang, M. Hu, J. Zhang, L. Li, and Z. Lin, "Design and optimization of load-independent magnetic resonant wireless charging system for electric vehicles," *IEEE Access*, vol. 6, pp. 17264–17274, 2018.

[12] J. Wang, S. L. Ho, W. N. Fu, and M. Sun, "Analytical design study of a novel Witricity charger with lateral and angular misalignments for efficient wireless energy transmission," *IEEE Trans. Magn.*, vol. 47, no. 10, pp. 2616–2619, Oct. 2011.

[13] Z. Dai, Z. Fang, H. Huang, Y. He, and J. Wang, "Selective omnidirectional magnetic resonant coupling wireless power transfer with multiple-receiver system," *IEEE Access*, vol. 6, pp. 19287–19294, 2018.

[14] Z. Dai, J. Wang, L. Jin, H. Jing, Z. Fang, and H. Hou, "A full-freedom wireless power transfer for spheroid joints," *IEEE Access*, vol. 7, pp. 18675–18684, 2019.

[15] J.-Y. Lee, L.-Y. Huang, and C.-Y. Chen, "Design and implementation of contactless maglev rotating power transfer system with new rotary inductive coupled structure," in *Proc. IEEE 8th Int. Power Electron. Motion Control Conf. (IPEMC-ECCE Asia)*, Hefei, China, May 2016, pp. 2442–2449.

[16] Y. Li, W. Ding, K. Song, and H. Bian, "A new type of in-wheel outer rotor switched reluctance motor drive based on selective wireless power transfer technology," in *Proc. 22nd Int. Conf. Electr. Mach. Syst. (ICEMS)*, Harbin, China, Aug. 2019, pp. 1–5.

[17] J. Kang, Y. Liu, and L. Sun, "A primary-side control method of wireless power transfer for motor electric excitation," in *Proc. 14th IEEE Conf. Ind. Electron. Appl. (ICIEA)*, Xi'an, China, Jun. 2019, pp. 2423–2428.

[18] A. Chiba, T. Fukao, and M. A. Rahman, "Vibration suppression of a flexible shaft with a simplified bearingless induction motor drive," *IEEE Trans. Ind. Appl.*, vol. 44, no. 3, pp. 745–752, May/Jun. 2008.

[19] H.-B. Gao, N. Sun, R.-Q. Zhang, Y. Ma, and Z.-B. Jia, "Dynamic analysis and study on Shaft's torsional vibration of electrical traction Shearer's motor-rocker and deceleration system," in *Proc. 2nd Int. Conf. Intell. Comput. Technol. Autom.*, Changsha, China, 2009, pp. 54–57.

[20] Z. Dai, J. Wang, M. Long, and H. Huang, "A Witricity-based high-power device for wireless charging of electric vehicles," *Energies*, vol. 10, no. 3, p. 323, Mar. 2017.

[21] N. Ha-Van and C. Seo, "Analytical and experimental investigations of omnidirectional wireless power transfer using a cubic transmitter," *IEEE Trans. Ind. Electron.*, vol. 65, no. 2, pp. 1358–1366, Feb. 2018.

[22] R.-J. Wang and M. J. Kamper, "Calculation of eddy current loss in axial field permanent-magnet machine with coreless stator," *IEEE Trans. Energy Convers.*, vol. 19, no. 3, pp. 532–538, Sep. 2004.

JIANGUI LI was born in Shanxi, China, in 1983. She received the Ph.D. degree from The University of Hong Kong. She joined the University of Michigan, as a Postdoctoral Researcher, in 2012. She is currently a Professor with the School of Mechanical and Electronic Engineering, Wuhan University of Technology. Her main research topics include wireless charging, electric motor, and renewable energy power generation.

HUI NIE received the M.A.Eng. degree from the Wuhan Institute of Technology, in 2018, where he is currently pursuing the Ph.D. degree. His main research interests include wireless transmission technology based on magnetic resonance, and system equipment for transmission and distribution.

JINCHENG LIU was born in Shandong, China, in 1995. He received the B.Eng. degree from Yantai University, in 2018. He is currently pursuing the M.A.Eng. degree with the Wuhan University of Technology. His main research interests include wireless power transfer technology based on magnetic resonance and motor structure, and industrial applications.

LONGYANG WANG received the B.Eng. degree from the Wuhan University of Technology, in 2017, where he is currently pursuing the Ph.D. degree. His main research interests include wireless transmission technology based on magnetic resonance, linear motor, and system equipment for transmission and distribution.

SHAOXING KE was born in Hubei, China, in 1995. He received the B.Eng. degree from the Tianjin University of Technology, in 2018. He is currently pursuing the M.A.Eng. degree with the Wuhan University of Technology. His main research interests include the high-precision speed control of permanent magnet synchronous motors and the advanced control strategies for high-performance electric drives.

• • •